Electronic Supplementary Material (ESI) for Nanoscale.


# Broadband Single-Molecule Fluorescence Enhancement Based on Self-Assembled Ag@Au Dimer Plasmonic Nano-antennas

Yunpeng Lin[a,b], Jinyong Hu[c], Wenbo Zhang[a,b], Li Jiang[d], Deqi Yi[a,b], Thitima Rujiralai[e], and Jie Ma*[a,b]

[a]School of Physics, Sun Yat-sen University, Guangzhou 510275, P. R. China.

[b]State Key Laboratory of Optoelectronic Materials and Technologies, Sun Yat-sen University, Guangzhou 510275, P. R. China.

[c]School of Physics and Optoelectronics, Xiangtan University, Xiangtan 411105, P. R. China.

[d]College of Science, Guilin University of Technology, Guilin 541004, P. R. China.

[e]Division of Physical Science, Faculty of Science, Prince of Songkla University, Hat Yai, Songkhla 90110, Thailand.

*Corresponding author. Email: majie6@mail.sysu.edu.cn

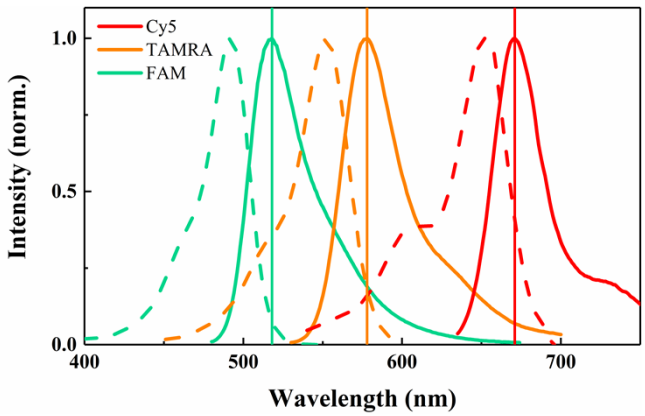


**Fig. S1** The absorption (dashed lines) and emission (solid lines) spectra of FAM (green), TAMRA (yellow), and Cy5 (red) with the indicated emission peaks at 520, 580 and 670 nm, respectively.

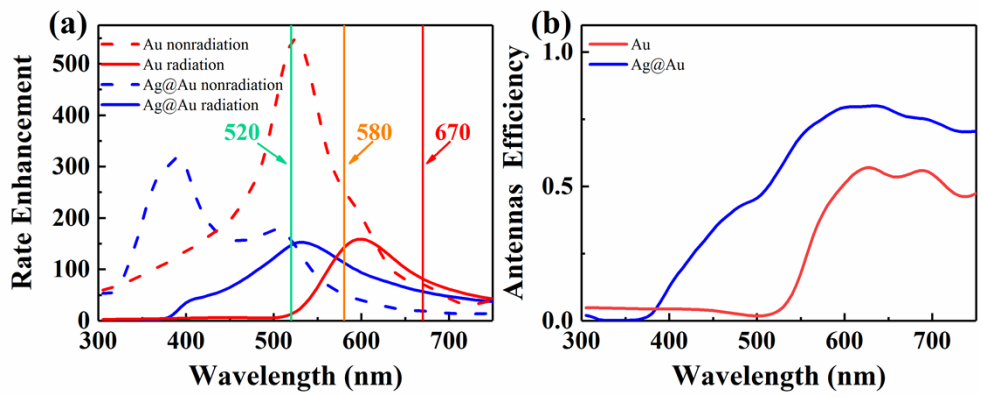


**Fig. S2** (a) Numerical simulations of radiation enhancement ($f_r$, solid lines) and non-radiation enhancement ($f_{nr}$, dashed lines) obtained for 70 nm Au (red) and Ag@Au (blue) (with 1 nm Au shell) dimer OAs as a function of the wavelength of emission light. The emission peaks of FAM (~520 nm), TAMRA (~580 nm) and Cy5 (~670 nm) are included as reference lines. (b) Numerical simulations of antenna efficiency ($\eta$) of Au and Ag@Au dimer OAs in UV-Visible spectral range.

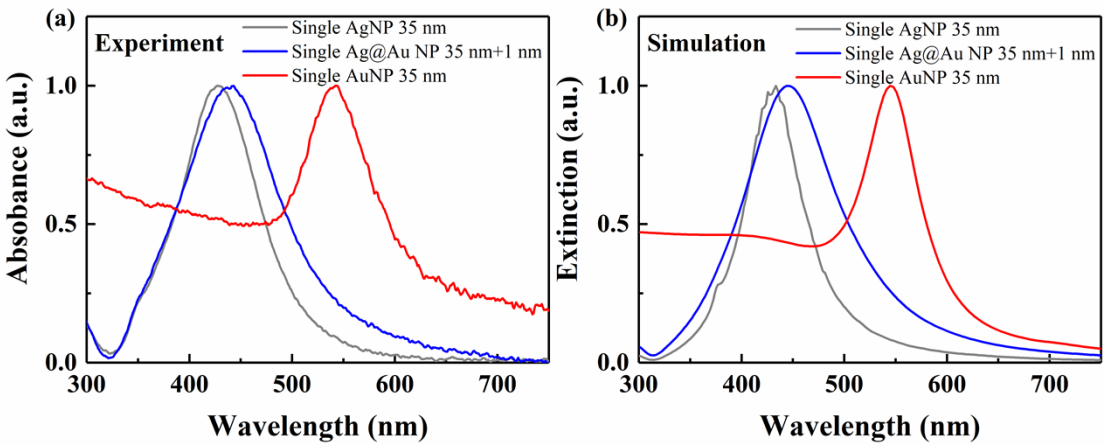


**Fig. S3** The extinction spectra of single AgNPs (radius *r*=35 nm, grey), Ag@Au NPs (*r*=35 nm for Ag core with an Au layer of 1 nm, blue) and AuNPs (*r*=35 nm, red) measured with a UV-Visible spectrophotometer (a) compared with the simulation results (b). The extinction peak of AgNPs shows a slight red-shift when coating with only 1 nm Au-shell (*i.e.*, Ag@Au NPs), the good consistency of experimental and simulated results supports that the Ag@Au NPs coated with an ultra-thin Au-shell were successfully synthesized.

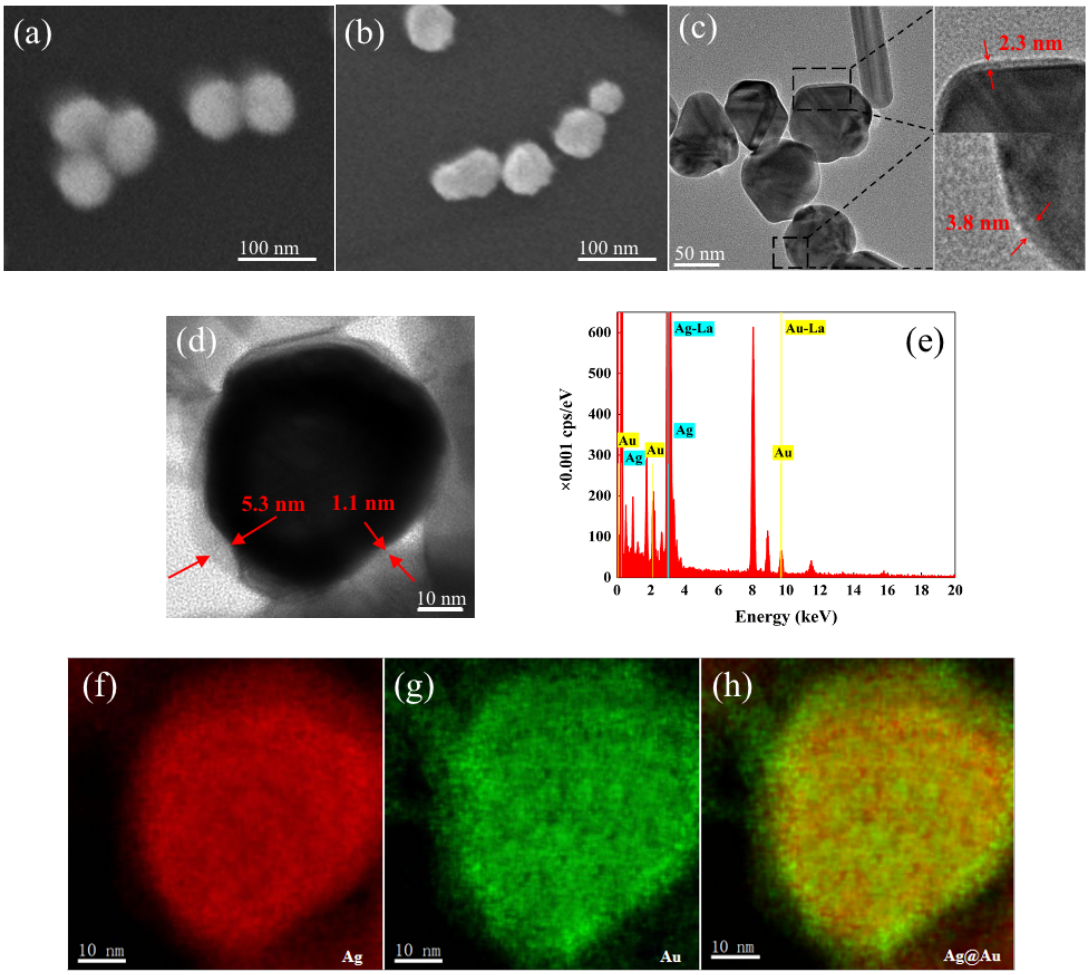


**Fig. S4** SEM images of Au (a) and Ag@Au (b) nanoparticles. (c) A bright field image of Ag@Au NPs from 300 kV HRTEM. There is a clear difference in the contrast at the edge of the nanoparticles, as indicated by the red arrows as examples. The thickness of the Au shell indicated by the red arrow is 2.3 nm and 3.8 nm, respectively. (d) In a typical bright field image, the contrast at the edge of the particle can be clearly seen, indicating a core-shell structure for the particle. The shell is not uniform and its thickness varies from ~1 nm to ~5 nm for different regions. (e) The EDS element analysis of the particle clearly shows that both Ag and Au are present in the particle as evidenced by the distinct peaks of Ag and Au elements. The other characteristic peaks are from Cu, C, O and Si elements which are caused by the copper mesh and the carbon film in the sample. The ratio of Ag and Au elements can be estimated from the indicated characteristic peaks (*i.e.*, "Ag-La" and "Au-

La") of Ag and Au, which is about 91.5%: 8.5%. (f)-(h) The mapping images from Ag elements or Au elements as well as the overlaid images from both Ag and Au elements. From the comparison of the three images, it can be seen that the distribution of Au element is wider than that of Ag element, which is consistent with the results from the bright field images and supports that the whole Ag NP is covered by Au and forms a core-shell structure.

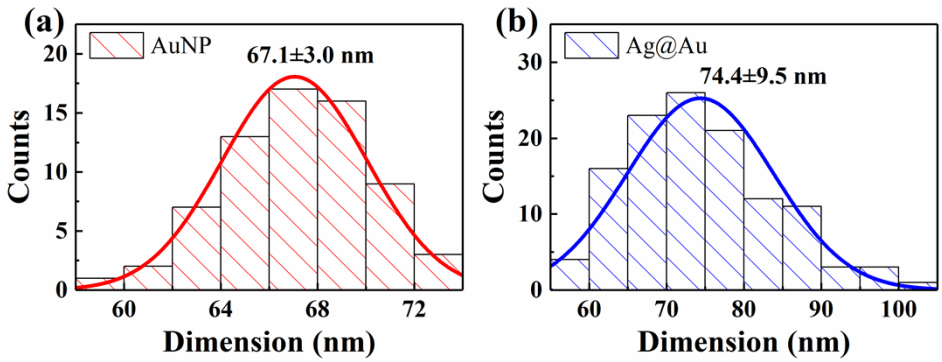


**Fig. S5** Population statistics of the sizes of Au (a) and Ag@Au (b) nanoparticles obtained from SEM. All the data are fitted with a Gaussian function with the values of mean sizes and standard errors indicated.

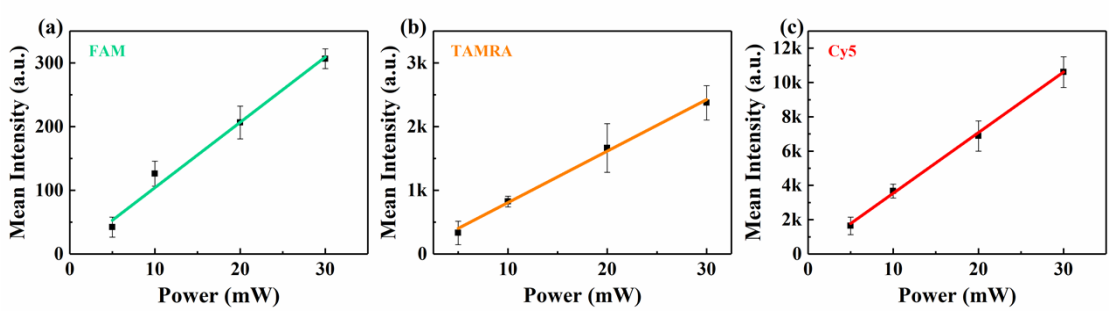


**Fig. S6** A saturation test of excitation power for three fluorescent dyes: (a) FAM, (b) TAMRA, and (c) Cy5. The calculated mean fluorescence intensities with error bars are obtained from SMF signals based on Au dimer OAs. For each dye molecule, the data are plotted with a linear fitting. Note that the power here represents the laser output power and the SMF signals were measured under TIRF mode. The good linear fitting indicates that the laser power used in our experiments is below the saturation threshold.

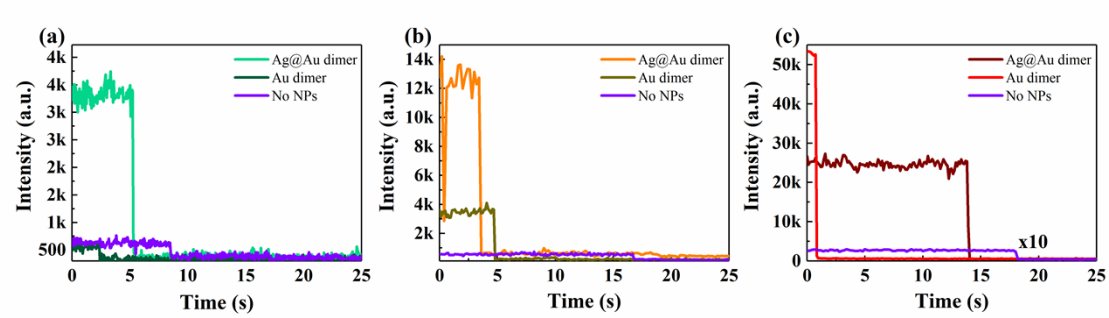


**Fig. S7** Three exemplary single-molecule fluorescence transients based on Au and Ag@Au dimer OAs as well as in the absence of OAs for three kinds of dyes: (a) FAM (excited at 488 nm), (b) TAMRA (excited at 561 nm), and (c) Cy5 (excited at 638 nm). In (c), for better visualization, the traces corresponding to the case of "No OAs" is plotted with 10-fold magnification as its original signal is too small to be seen under the current scale. The trace (red line) in (c) corresponds to the largest enhanced fluorescence signal measured in our experiments and the enhancement reaches ~175-fold.

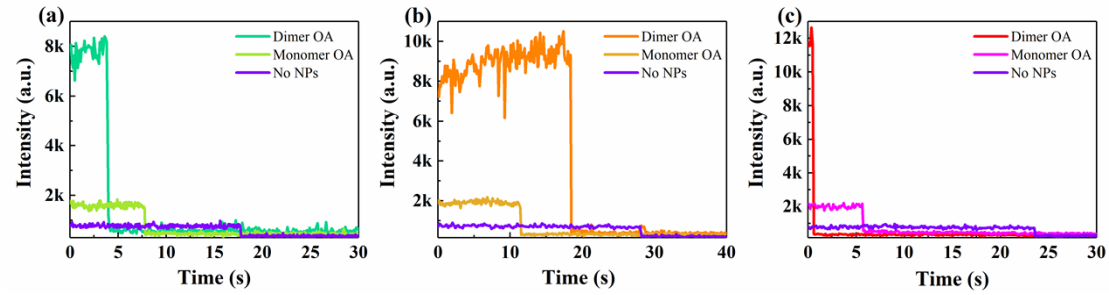


**Fig. S8** Typical single-molecule fluorescence transients based on Ag@Au dimer and monomer OAs as well as in the absence of OAs are plotted together for three different dyes: (a) FAM (excited at 488 nm), (b) TARAM (excited at 561 nm), and (c) Cy5 (excited at 638 nm).

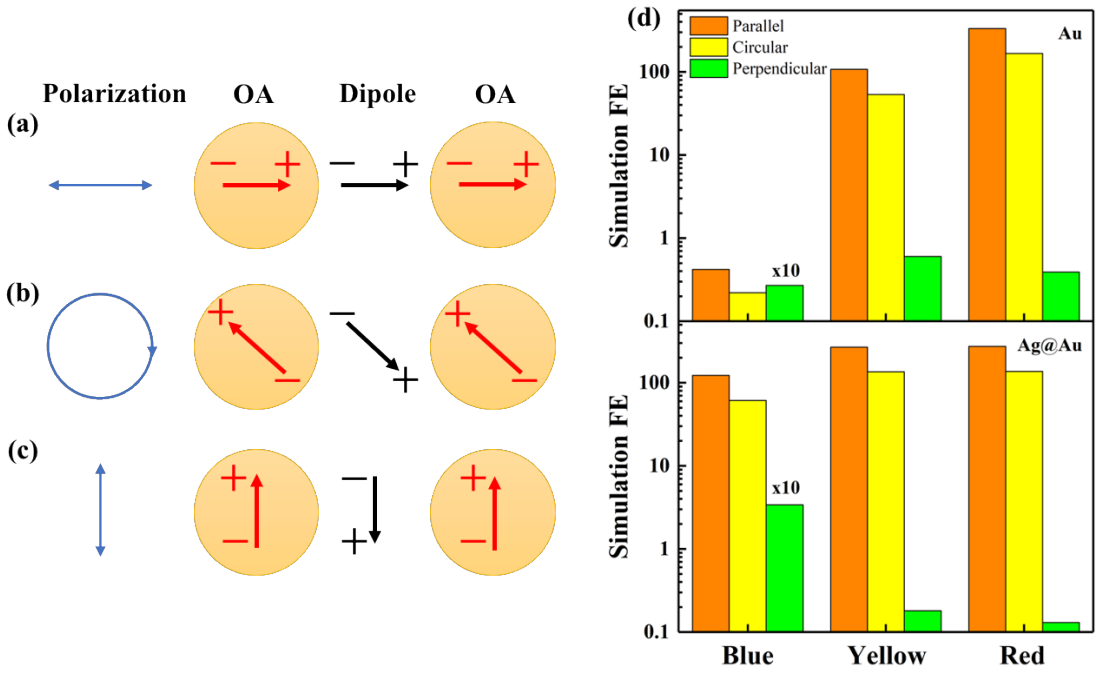


**Fig. S9** Sketch of surface charge of a fluorophore on the OA element induced by the different polarization of incident light. Three different polarization modes are shown as follows: (a) linear polarization parallel to the orientation of a dimer OA; (b) circular polarization; (c) linear polarization perpendicular to the orientation of a dimer OA. Note that the red arrows represent the induced dipoles in the NPs, while the black arrows represent the emission dipole moment of the fluorophore. (d) Numerical simulation of maximum FE (orange histograms, corresponding to parallel excitation in (a)) and mean FE (yellow histograms, corresponding to circular excitation in (b)) as well as minimum FE (green histograms, corresponding to perpendicular excitation in (c)) for 70 nm Au (upper panel) and Ag@Au (lower panel) dimer OAs. For better visualization, all of the values are plotted logarithmically and the minimum FEs corresponding to the perpendicular excitation in blue region for Au and Ag@Au dimer OA are plotted with 10-fold magnification.

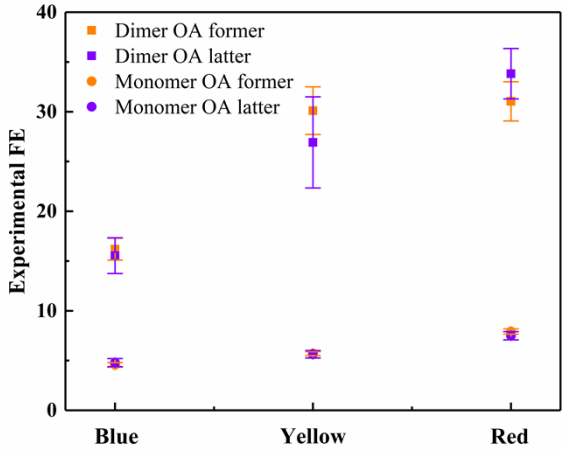


**Fig. S10** The measured broadband fluorescence enhancements for Ag@Au OAs before and more than one month later. The measured FEs are consistent with each other, indicating that the Ag@Au NPs remain stable for more than one month and their performance in broadband fluorescence enhancement is not compromised at all.

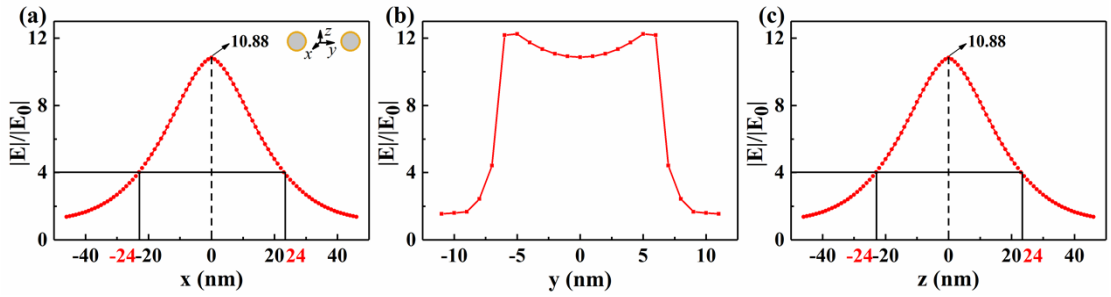


**Fig. S11** Numerical simulations of the electric field enhancement distribution along (a) x-direction; (b) y-direction; (c) z-direction. The excitation light used here is 561 nm and circularly polarized (see Fig. 2(e)). Note that here the origin of the coordinate system is set at the center of the interparticle gap (*i.e.*, the "hotspot") and the value of 10.88 represents the electric field intensity enhancement at the hotspot. As can be seen in (a) and (c), the electric field intensity enhancement quickly decays when $|x|$ or $|z|$ increases, and it drops to 4 at $|x|$ or $|z|$=24 nm, which is 1/e times of that at the center. Based on the simulation results above, the excitation volume of self-assembled Ag@Au dimer OA can be estimated to be $V = 48 \times 48 \times 14\ (nm^3) \approx 32\ zL$.

**The description of the revised model**

We first consider a 2D model in which both two metallic NPs are immobilized on the surface so that the orientation of the dimer OA is within x-y plane. Given the angle ($\varphi$) of excitation polarization relative to the dimer OA orientation, the fluorescence enhancement (FE) can be expressed as:

$$\mathrm{FE} = FE_{max}\cos^2\varphi \qquad (S1)$$

where $FE_{max}$ is the maximum FE when the linearly polarized light is parallel to the orientation of dimer OA. If the orientation of the dimer OA is random or the excitation light is circularly polarized, a mean FE could be obtained as follows:

$$FE_{avg} = \frac{4}{2\pi}\int_0^{\frac{\pi}{2}} FE_{max}\cos^2\varphi d\varphi = \frac{1}{2}FE_{max} \qquad (S2)$$

It means that for these cases, we could get a mean FE equaling to a half of maximum FE (see Fig. S9).

In our experiment, we employed a linearly polarized light to excite fluorescent dyes. The orientation of dimer OAs is also random in three-dimensions rather than x-y plane. Therefore, it is necessary to consider a revised 3D model to consider all these factors in order to be more accurate. To do this, besides the polar angle $\varphi$, we then introduce another parameter $\theta$ as azimuthal angle to describe the 3D orientation of a dimer OA, as shown in Fig. 6(a). According to a previous study,[S1] the fluorescence intensity $I_f \propto |p \cdot E|^2 \propto \cos^2\beta = \cos^2\varphi\sin^2\theta$, where $p$ is the dipole moment of the molecule, $E$ is the excitation electric field, and $\beta$ is the angle between $p$ and $E$. Hence given a specific configuration for the dimer OA and excitation light, FE in this revised 3D model can be written as:

$$\mathrm{FE} = FE_{max}\cos^2\beta = FE_{max}\cos^2\varphi\sin^2\theta \qquad (S3)$$

On the other hand, due to the TIRF illumination mode, the excitation field intensity decays

exponentially along the z-axis, *i.e.*,

$$E_t = E_0 e^{-\gamma z} e^{-i(\omega t - k_y y)} \quad (S4)$$

where $\gamma$ is a decay constant, $\omega$ and $k_y$ represent the frequency and wave vector of excitation light, respectively. Then $\gamma$ can be expressed as $\gamma = \frac{2\pi}{\lambda_0}\sqrt{n_i^2 \sin^2\theta_i - n_t^2}$. Here $\lambda_0$ is the vacuum wavelength, $\theta_i$ is the incident angle of the excitation light, $n_i$ and $n_t$ are the refractive index of glass and aqueous solution, respectively. Here we assume that the effect of antennas on evanescent wave can be neglected. We then define $d_z = 1/\gamma$ as depth of penetration. Consequently, the excitation power distribution along z-axis can be described as:

$$I(z) = |E_t|^2 = I_s e^{-\frac{2z}{d_z}} \quad (S5)$$

where $I_s$ is the excitation power at the surface of glass coverslip (*i.e.*, z=0). The dye molecule thus locates at $z = r_0 + \frac{l}{2} * \cos\theta$ as shown in Fig. 6(a), where $r_0$ is a radius of Au or Ag@Au nanoparticle and $l$ is the distance between the centers of the two spheres. Since we have proved that fluorescence intensity is in proportion to excitation power (see Fig. S6), then $FE$ under the TIRF excitation mode can be written as:

$$\mathrm{FE} = FE_{max} \cos^2\varphi \sin^2\theta e^{-\frac{2r_0 + l * \cos\theta}{d_z}} \quad (S6)$$

In the end, the mean FE based on this model can be obtained as follows:

$$FE_{avg} = FE_{max} \cdot \frac{1}{2\pi} \int_0^{2\pi} \cos^2\varphi d\varphi \int_0^{\frac{\pi}{2}} \sin^3\theta e^{-\frac{2r_0 + l * \cos\theta}{d_z}} d\theta \quad (S7)$$

To calculate the integral above, we set $k = l/d_z$. The mean FE thus can be expressed as a function of $k$:

$$FE_{avg} = \frac{FE_{max}}{2} \cdot e^{-\frac{2r_0}{d_z}} \left[\frac{1}{k} + \frac{2}{k^2} e^{-k} + \frac{2}{k^3} e^{-k} - \frac{2}{k^3}\right] \quad (S8)$$

In our experiment, $l = 84\ nm$, $d_z \sim 200\ nm$, we thus obtain $k = 0.42$ and then substitute it into

equation S(8). Ultimately, we can obtain $FE_{avg} \approx 0.20FE_{max}$.

In addition, when ignoring the influence of TIRF mode-caused power decay, the mean FE is given by the following equation:

$$FE_{avg} = FE_{max} \cdot \frac{1}{2\pi}\int_0^{2\pi} \cos^2 \varphi d\varphi \int_0^{\frac{\pi}{2}} \sin^3 \theta d\theta = \frac{1}{3}FE_{max} \qquad (S9)$$

**Table S1** The modified DNA sequences used in the experiments

| Name | Name | Sequence (5′ to 3′) | Modification |
|---|---|---|---|
| | **ssDNA-C** | GCA CGA AAC CTG GAC TAG ATG GGA ACA GCA | 5′ end: triple thiol; T-Cy5 |
| **ssDNA-1** | **ssDNA-T** | GCA CGA AAC CTG GAC TAG ATG GGA ACA GCA | 5′ end: triple thiol; T-TAMRA |
| | **ssDNA-F** | GCA CGA AAC CTG GAC TAG ATG GGA ACA GCA | 5′ end: triple thiol; T-FAM |
| **ssDNA-2** | | TGC TGT TCC CAT CTA GTC CAG GTT TCG TGC | 5′ end: triple thiol |

**Table S2** Intrinsic quantum yield of dyes ($\phi^0$), antenna efficiency ($\eta$), radiation enhancement ($f_r$) with corresponding emission enhancement factor $(EF_{em})$, excitation enhancement factor ($EF_{ex}$), mean fluorescence enhancement ($FE_{avg}$) obtained for different dimer OAs from numerical simulations

| | ***Dye*** | $\phi^0$ | $\eta$ | $f_r$ | $EF_{em}$ | $EF_{ex}$ | $FE_{avg}$ |
|---|---|---|---|---|---|---|---|
| **Au (*r*=35 nm)** | Cy5 | 0.27[S2] | 0.59 | 127.10 | 2.16 | 92.66 | 199.97 |
| | TAMRA | 0.60[S3] | 0.40 | 243.85 | 0.67 | 87.03 | 57.96 |
| | FAM | 0.81[S4] | 0.039 | 30.27 | 0.043 | 5.39 | 0.23 |
| **Ag (*r*=35 nm)** | Cy5 | 0.27 | 0.70 | 86.83 | 2.54 | 52.09 | 132.17 |
| | TAMRA | 0.60 | 0.80 | 143.63 | 1.33 | 86.89 | 115.42 |
| | FAM | 0.81 | 0.86 | 243.85 | 1.06 | 127.63 | 135.40 |
| **Ag (*r*=35 nm) Au-shell (1 nm)** | Cy5 | 0.27 | 0.74 | 96.20 | 2.68 | 60.64 | 162.81 |
| | TAMRA | 0.60 | 0.73 | 195.01 | 1.21 | 118.10 | 143.33 |
| | FAM | 0.81 | 0.55 | 251.51 | 0.68 | 99.33 | 67.41 |
| **Ag (*r*=35 nm) Au-shell (3 nm)** | Cy5 | 0.27 | 0.71 | 123.68 | 2.63 | 79.60 | 208.98 |
| | TAMRA | 0.60 | 0.63 | 250.52 | 1.05 | 139.42 | 145.96 |
| | FAM | 0.81 | 0.30 | 190.46 | 0.37 | 53.45 | 19.79 |
| **Ag (*r*=35 nm) Au-shell (5 nm)** | Cy5 | 0.27 | 0.72 | 155.26 | 2.63 | 100.96 | 265.89 |
| | TAMRA | 0.60 | 0.59 | 275.69 | 0.98 | 138.19 | 135.69 |
| | FAM | 0.81 | 0.19 | 137.10 | 0.23 | 31.46 | 7.38 |
| **Au (*r*=40 nm)** | Cy5 | 0.27 | 0.67 | 199.81 | 2.46 | 133.87 | 329.32 |
| | TAMRA | 0.60 | 0.41 | 215.38 | 1.02 | 78.00 | 79.56 |
| | FAM | 0.81 | 0.036 | 28.29 | 0.044 | 5.01 | 0.22 |

**Table S3** Characteristic photobleaching rate ($k$) with corresponding standard error ($SE$), characteristic photobleaching time ($\tau_b$) obtained from the photobleaching time under different situations (*i.e.*, "Dimer", "Monomer", "No NPs")

| | **Dimer** | | | **Monomer** | | | **No NPs** | | |
|---|---|---|---|---|---|---|---|---|---|
| | ***k* ($s^{-1}$)** | ***SE*** | **$\tau_b$(s)** | ***k* ($s^{-1}$)** | ***SE*** | **$\tau_b$(s)** | ***k* ($s^{-1}$)** | ***SE*** | **$\tau_b$(s)** |
| **Cy5** | 0.17 | 0.04 | 5.86 | 0.25 | 0.02 | 3.93 | 0.05 | 0.01 | 18.48 |
| **TAMRA** | 0.12 | 0.03 | 8.16 | 0.09 | 0.03 | 10.83 | 0.03 | 0.01 | 38.85 |
| **FAM** | 0.23 | 0.07 | 4.32 | 0.21 | 0.04 | 4.74 | 0.18 | 0.06 | 5.49 |

**Table S4** Values of peak center ($x_c$) and width ($w$), mean values ($\mu$) with corresponding standard deviation ($\sigma$) and standard error ($SE$) obtained from Au and Ag@Au OA FE histogram fitted with a log-normal distribution

| | | **Dimer** | | | | | **Monomer** | | | | |
|---|---|---|---|---|---|---|---|---|---|---|---|
| | | $x_c$ | $w$ | $\mu$ | $\sigma$ | $SE$ | $x_c$ | $w$ | $\mu$ | $\sigma$ | $SE$ |
| **Au** | Cy5 | 49.88 | 0.22 | 51.10 | 23.62 | 1.97 | 19.36 | 0.42 | 21.15 | 4.49 | 0.52 |
| | TAMRA | 12.57 | 0.41 | 13.92 | 12.17 | 1.27 | 4.30 | 0.23 | 4.44 | 0.83 | 0.13 |
| | FAM | 0.32 | 0.30 | 0.34 | 0.10 | 0.02 | 0.73 | 0.16 | 0.74 | 0.11 | 0.01 |
| **Ag@Au** | Cy5 | 23.61 | 0.74 | 31.05 | 17.94 | 1.97 | 7.73 | 0.22 | 7.92 | 3.22 | 0.26 |
| | TAMRA | 20.98 | 0.85 | 30.11 | 25.12 | 2.40 | 5.45 | 0.30 | 5.70 | 2.24 | 0.20 |
| | FAM | 14.37 | 0.49 | 16.20 | 8.69 | 1.10 | 4.50 | 0.17 | 4.57 | 1.99 | 0.23 |

**References:**


S1 A. Mohammadi, V. Sandoghdar, M. Agio, *New J. Phys.,* 2008, **10**, 105015.

S2 K. Hübner, M. Pilo-Pais, F. Selbach, T. Liedl, P. Tinnefeld, F. D. Stefani, G. P. Acuna, *Nano Lett.,* 2019, **19**, 6629-6634.

S3 M. V. Kvach, I. A. Stepanova, I. A. Prokhorenko, A. P. Stupak,V. V. Shmanai, *Bioconjugate Chem.,* 2009, **20**, 1673-1682.

S4 T. Mineno, T. Ueno, Y. Urano, H. Kojima, T. Nagano, *Org. Lett.,* 2006, **8**, 5963-5966.